A mutation associated with centronuclear myopathy enhances the size and stability of dynamin 2 complexes in cells

Nicholas G. James [a], Michelle A. Digman [b], Justin A. Ross [a,1], Barbara Barylko [c], Lei Wang [c], Jinhui Li [d], Yan Chen [d], Joachim D. Mueller [d], Enrico Gratton [b], Joseph P. Albanesi [c], David M. Jameson [a,*]

[a] Department of Cell and Molecular Biology, John A. Burns School of Medicine, University of Hawaii, 651 Ilalo Street, Biosciences 222, Honolulu, HI 96813, USA
[b] Laboratory for Fluorescence Dynamics, Department of Biomedical Engineering, University of California, Irvine, CA 92697, USA
[c] Department of Pharmacology, University of Texas Southwestern Medical Center, 5323 Harry Hines Blvd., Dallas, TX 75390-9041, USA
[d] School of Physics and Astronomy, University of Minnesota, Minneapolis, MN 55455, USA

ABSTRACT

Background: Dynamin 2 (Dyn2) is a ~100 kDa GTPase that assembles around the necks of nascent endocytic and Golgi vesicles and catalyzes membrane scission. Mutations in Dyn2 that cause centronuclear myopathy (CNM) have been shown to stabilize Dyn2 polymers against GTP-dependent disassembly in vitro. Precisely timed regulation of assembly and disassembly is believed to be critical for Dyn2 function in membrane vesiculation, and the CNM mutations interfere with this regulation by shifting the equilibrium toward the assembled state.
Methods: In this study we use two fluorescence fluctuation spectroscopy (FFS) approaches to show that a CNM mutant form of Dyn2 also has a greater propensity to self-assemble in the cytosol and on the plasma membrane of living cells.
Results: Results obtained using brightness analysis indicate that unassembled wild-type Dyn2 is predominantly tetrameric in the cytosol, although different oligomeric species are observed, depending on the concentration of expressed protein. In contrast, an R369W mutant identified in CNM patients forms higher-order oligomers at concentrations above 1 μM. Investigation of Dyn2-R369W by Total Internal Reflection Fluorescence (TIRF) FFS reveals that this mutant forms larger and more stable clathrin-containing structures on the plasma membrane than wild-type Dyn2.
Conclusions and general significance: These observations may explain defects in membrane trafficking reported in CNM patient cells and in heterologous systems expressing CNM-associated Dyn2 mutants.

© 2013 Elsevier B.V. All rights reserved.

1. Introduction

Centronuclear myopathies (CNM) are congenital disorders characterized clinically by muscle weakness and wasting and morphologically by the presence of chains of centralized nuclei in muscle fibers (reviewed in [1,2]). The majority of CNM cases have been linked to mutations in proteins implicated in membrane trafficking pathways [3].

These proteins include myotubularin, associated with an X-linked form of the disease [4], Bin1/amphiphysin 2, associated with an autosomal recessive form [5], and dynamin 2 (Dyn2), the protein investigated in this study and responsible for most known autosomal dominant forms of CNM [6].

Dynamins (Dyns) are ~100 kDa GTPases involved in membrane fission during vesicle formation (recently reviewed in [7–10]). They have been most extensively characterized as mediators of endocytosis, a role first described by van der Bliek and Meyerowitz [11], but they also participate in Golgi budding [12], phagocytosis [13], and organization of the actin cytoskeleton [14]. Three dynamin isoforms, Dyn1, Dyn2, and Dyn3, are expressed in mammals, with each isoform containing multiple splice variants [15]. Dyn1 is expressed primarily in presynaptic nerve terminals, where it functions in synaptic vesicle recycling [16]. Dyn2 is ubiquitously expressed and accounts for most of the dynamin functions that are not specifically related to synaptic vesicle retrieval after exocytosis; and Dyn3 is enriched in the testes, lung and brain, where its precise functions remain to be elucidated. All three dynamin isoforms contain five functional domains: an N-terminal GTPase domain; a middle domain that participates in dynamin self-association; a Pleckstrin

Homology (PH) domain involved in phosphoinositide binding; a GTPase effector domain (GED), which interacts with the GTPase domain [17] in a manner that stimulates catalytic activity [18]; and a C-terminal proline/arginine-rich domain (PRD), which mediates most interactions between dynamins and other proteins. Four mutations (E368K, R369W, R369Q, and R465W) affecting three middle domain residues were originally linked to Dyn2-dependent CNM [6]. Additional mutations have been localized to residues in the PH domain (R522C/H, R523G, E560K, D614N, A618D/T, S619L/W, L621P), in the PH domain-GED linker region (V625del and P627H/R), and in the GED (E650K) [19] (Fig. 1). In addition to these mutations, a non-overlapping set of mutations in dynamin 2 have been linked to Charcot-Marie-Tooth neuropathies [19].

Dynamins catalyze membrane fission by assembling around the necks of budding vesicles, thereby constricting and severing these necks in a process that is tightly coupled to GTP hydrolysis. The self-assembly and GTP-dependent disassembly of Dyn polymers have been characterized in vitro, primarily by monitoring changes in turbidity and/or sedimentation. Using these methods, we showed that CNM mutations in the middle domain (E368K, R369W, and 465 W) and PH domain (A618T) enhance Dyn2 polymerization, stabilize Dyn2 polymers against GTP-dependent disassembly and, as a result of this stabilization, increase Dyn2 GTPase activity [20]. Enhanced Dyn1 GTPase activity due to CNM-linked PH domain mutations was also reported by Kenniston and Lemmon [21]. In the present study we use fluorescence fluctuation spectroscopy (FFS) approaches to examine how the R369W mutation affects the behavior of Dyn2 in the cytosol and plasma membrane of living cells. This mutation accounts for ~10% of known cases of autosomal dominant CNM [19], and was recently shown to induce histopathological changes in extraocular muscles [22].

2. Materials and methods

2.1. Materials

NaCl, HEPES, PIPES, $MgCl_2$, NADH, EDTA, GTP (sodium salt) and phenylmethylsulfonyl fluoride (PMSF) were all from Sigma-Aldrich (St. Louis, MO, USA). KCl was from Fluka (St. Louis, MO, USA). Amicon Ultracell-4 10 kDa MWCO filters were from Millipore (Billerica, MA, USA). Male African green monkey cells (CV1), human osteosarcoma (U2OS) cells, Eagle's Minimum Essential Medium (EMEM) and Fetal bovine serum (FBS) were purchased from ATCC (Manassas, VA, USA). Lipofectamine 2000, trypsin and mouse embryo fibroblast (MEF) cells were from Invitrogen (Carlsbad, CA, USA). TransFectin reagent was from Bio-Rad (Hercules, CA). DTT was from Fisher (Pittsburgh, PA, USA). Dulbecco's modified Eagle's medium (DMEM) and penicillin/streptomycin were from Gibco (Carlbad, CA, USA).

2.2. Constructs and protein expression

Wild-type (wt) Dyn2-EGFP and the CNM-associated Dyn2 mutant, R369W-EGFP were generated by inserting the corresponding constructs with C-terminal His_6 tags [20], into the pEGFP-N1 vector (Clontech). This EGFP construct contains F64L and S65T mutations to reduce self-association. Clathrin light chain a (LCa)-mCherry was constructed by introducing the LCa into the pmCherry-N1 vector (Clontech).

2.3. Cell culture

CV1 cells were cultured in EMEM supplemented with 10% FBS. MEFs and U2OS cells were cultured in high glucose DMEM supplemented with 10% FBS, 1% penicillin/streptomycin and 20 mM HEPES buffer. For imaging experiments, cells were grown at 37 °C in 5% CO_2 and transfected with wt-Dyn2-EGFP or R369W-EGFP alone, or together with LCb-mCherry, using Lipofectamine 2000 according to the manufacturer's protocol. After 24 h of transfection, cells were trypsinized, and plated alone (CV1) or on 2 μg/ml fibronectin-coated dishes (MEF) 2–3 h prior to imaging. For brightness analysis, U2OS cells were subcultured into eight-well coverglass chamber slides (Nalge Nunc International, Rochester, NY) two days before measurement. Transfection was carried out using TransFectin reagent according to the manufacturer's instructions 24 h before measurements.

2.4. Transmission Electron Microscopy (TEM)

WT-Dyn2 and the R369W mutant containing C-terminal His_6 tags were expressed in Sf9 cells and purified over Ni^{2+}-nitriloacetic acid resin [23]. Purified proteins were dialyzed against 20 mM HEPES (pH 7.5), 300 mM NaCl, 3 mM $MgCl_2$, 1 mM EDTA, 0.5 mM DTT and 0.2 mM PMSF. Aliquots were frozen and stored at −80 °C. Immediately before use, samples were centrifuged at 213,000 ×g for 20 min to remove aggregated protein. For electron microscopy, the cleared Dyn2 and R369W samples were diluted into 20 mM HEPES, pH 7.5 and 50 mM NaCl to a final protein concentration of 1 μM. After 30 s, Dyns were added to Formvar-coated 200 mesh copper grids, incubated for a further 30 s, and stained with 2% uranyl acetate for 60 s. To examine the effect of GTP on the stability of Dyn2 polymers, proteins were incubated with 1 mM MgGTP for 5 min prior to addition to grids. The grids were washed and dried before viewing on an LEO 912 energy filtering TEM (EFTEM) (Ziess, Oberkochen, Germany) at an accelerating voltage of 100 kV. Images were captured with a Proscan slow-scan fast-transfer 1 k × 1 k CCD.

2.5. Confocal images

Images where recorded on an Olympus Fluoview FV1000 confocal laser scanning microscope mounted on an Olympus IX-81 inverted microscope using a 60× 1.35 NA oil objective. Both Dyn2-EGFP and R369W-EGFP were excited at 488 nm with an Ar-Ion laser (Melles Griot, Carlsbad, CA) and fluorescence intensity was collected through a Q500LP dichroic mirror in front of the PMT.
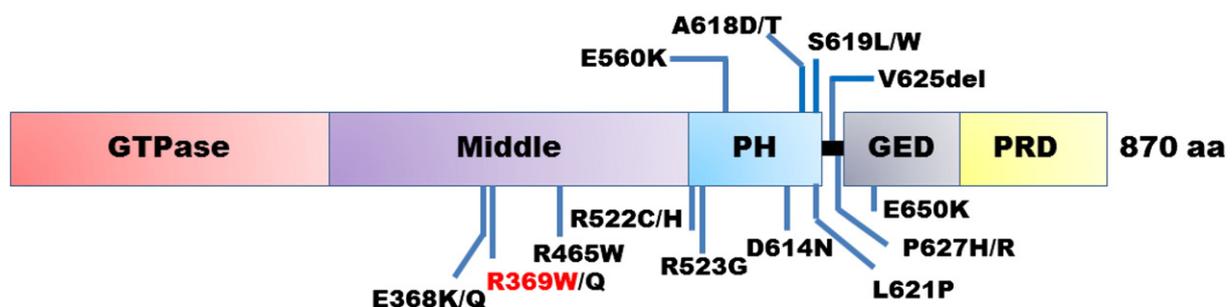

Fig. 1. Domain map of Dyn2 showing sites of CNM mutations; the R369W mutation is highlighted in red. Numbering refers to the dynamin 2 isoform 1, 870 aa, GI:56549121 variant.

2.6. Total Internal Reflection Fluorescence Microscopy

Images were taken on an Olympus IX-81 Total Internal Reflection Fluorescence (TIRF) microscope using a 60× 1.45 NA oil objective. A Cascade 512B EMCCD camera (Photometrics, Tucson, AZ) equipped with a dual view image splitter was used to image EGFP and mCherry proteins at 100 frames/s. Both proteins were excited simultaneously at 488 nm for EGFP and at 543 nm for mCherry at less than 10% laser power. Cells were imaged in a humidified enclosed chamber kept at 37 °C and with 5% CO_2 (Tokai Hit, Fujinomiya, Sizuoka, Japan). An objective heater wrapped round the neck of the objective was used to minimize temperature drifts (with a 20 minute delay to equilibrate the temperature prior to imaging) and the collar of the objective was adjusted to compensate for temperature and thickness of the coverslip.

2.7. Image analysis

Image correlation spectroscopy (ICS) and the Number and Brightness (N&B) method were used to analyze TIRF images. All image analyses were performed using SimFCS (E. Gratton, Laboratory for Fluorescence Dynamics, University of California Irvine). The average sizes of the puncta in a given field were determined using ICS analysis [24]. ICS is capable of determining size based on the standard deviation associated with the spatial autocorrelation function (ACF), which is calculated using the equation:

$$G_S(\xi, \psi) = \frac{\langle I(x,y) I(x+\xi, y+\psi) \rangle_{x,y}}{\langle I(x,y) \rangle_{x,y}^2}$$

where ξ and ψ are the spatial increments in the x and y directions, respectively, and the angle brackets indicate average over all the spatial locations in both x and y directions. Images were 256 × 256 pixels and the size of each pixel was determined by a Ronchi ruling.

TIRF images were obtained using dual-color microscopy. For the dual-color microscopy approach to work, the two images must be superimposed accurately (within a pixel). We studied the distortions of the optics and the zoom set (zoom 2 and 1.45 OIL TIRF Olympus objective) and found that a rigid rotation–translation is sufficient to make all points of the field of view coincident within one pixel in the two channels. For the z-direction, when the TIRF condition is achieved in both channels, the points are coincident and a diffraction limited spot gives a similar size in both channels. Thus the differences in size in this test case are only due to the different wavelengths of light rather than out-of-focus effects.

The N&B method was utilized to monitor the Number and Brightness of puncta. N&B analysis measures the average intensity and the variance of the intensity fluctuations at each pixel due to diffusion into or out of the focal volume. These parameters allow for the calculation of the number of particles (N) within the focal spot and the intrinsic brightness (B) of each particle. For an EMCCD camera, N and B are defined as [25]:

$$N = \frac{(\langle I \rangle - offset)^2}{\sigma^2 - \sigma_0^2} \quad ; \quad B = \frac{\sigma^2 - \sigma_0^2}{\langle I \rangle - offset}$$

where <I> is the average signal intensity, σ^2 is the variance, σ_0^2 is the readout noise variance of the detection electronics and offset is the intensity offset. We note that this method has been described for molecular events due to fast diffusion of molecules, [26] but has not been exploited for the determination of fluctuations arising from binding-unbinding processes. For the analysis carried out in this investigation we developed normalization tools that allowed us to determine the average size of the intensity fluctuations. This analysis is different from the normalized ratio at one pixel. The N&B analysis provides the average size of the fluctuation but not the time course of the fluctuations. However, this analysis is very fast and provides the statistics for every

punctum of the image simultaneously. If the punctum is stable, there are no fluctuations and the B parameter will only report the fluctuations due to the detector.

2.8. Measurement of dynamin oligomerization in the cytoplasm

The instrumentation for brightness analysis fluorescence fluctuation experiments has been described previously [27]. An excitation wavelength (for two-photon excitation) of 1000 nm is used for all experiments. Brightness is calculated with Q-analysis [28]. Monomer brightness of EGFP is obtained by averaging over 5 cells at various concentrations. The resulting normalized brightness, b, is calculated by taking the brightness of an individual measurement divided by the brightness of monomeric EGFP.

3. Results

3.1. The CNM-associated R369W mutation stabilizes Dyn2 rings in the presence of GTP

We first wished to ascertain that the stable polymers of Dyn2-R369W, which we had previously examined using turbidity assays [20], were similar in overall structure to those formed by wt-Dyn2, and not merely random aggregates. Upon dilution into low ionic strength buffer, wt-Dyn2 self-assembles into rings and small stacks of rings ([29]; Fig. 2A). Similar structures were formed by Dyn2-R369W upon reduction of NaCl concentration from 300 mM to 50 mM, although the darker staining of the R369W rings suggested that they were somewhat larger in the Z-direction than wt-Dyn2 rings (Fig. 2B). Consistent with our earlier observations [20], R369W polymers were more resistant to destabilization by GTP than wt-Dyn2 polymers, as ring structures remained clearly visible even in the presence of nucleotide (Fig. 2D), whereas addition of GTP to wt-Dyn2 caused complete dissociation of ring structures (Fig. 2C).

3.2. Association of Dyn2-R369W with large cytoplasmic particles

In the course of these studies we noted that R369W-EGFP formed large cytoplasmic inclusions (as evident by conventional confocal fluorescence microscopy shown in Fig. 3), which were far less prominent in cells expressing wt-Dyn2-EGFP. Interestingly, large intracellular accumulations of Dyn2 and dysferlin were observed in muscle fibers from heterozygous knock-in mice expressing wt-Dyn2 and the CNM-associated R465W mutant at approximately endogenous levels [30]. CNM Dyn2 mutants R465W and S619L were also identified in enlarged clathrin-positive structures, similar in appearance to those shown here, when overexpressed in COS-1 cells [31]. Although the relationship between these structures and our R369W-containing inclusions is unclear at present, these results provide further evidence that CNM mutations induce the formation of inordinately large Dyn2-containing complexes in cells.

3.3. The R369W mutation enhances oligomerization of unassembled Dyn2 in the cytoplasm of living cells

The primary objective of this study was to determine how the R369W mutation affects the self-assembly of Dyn2 in living cells. We first asked whether this mutation influences the oligomeric state of unassembled Dyn2 in the cytosol. Previous in vitro studies aimed at defining the size of the minimal dynamin assembly unit have yielded conflicting results. For example, our sedimentation equilibrium measurements in the analytical ultracentrifuge indicated that all three forms of dynamin exist predominantly as monomer–tetramer or monomer–dimer–tetramer equilibria in solutions containing 300 mM NaCl [32–34]. The R369W mutation did not significantly alter sedimentation behavior of Dyn2 [20]. In contrast,
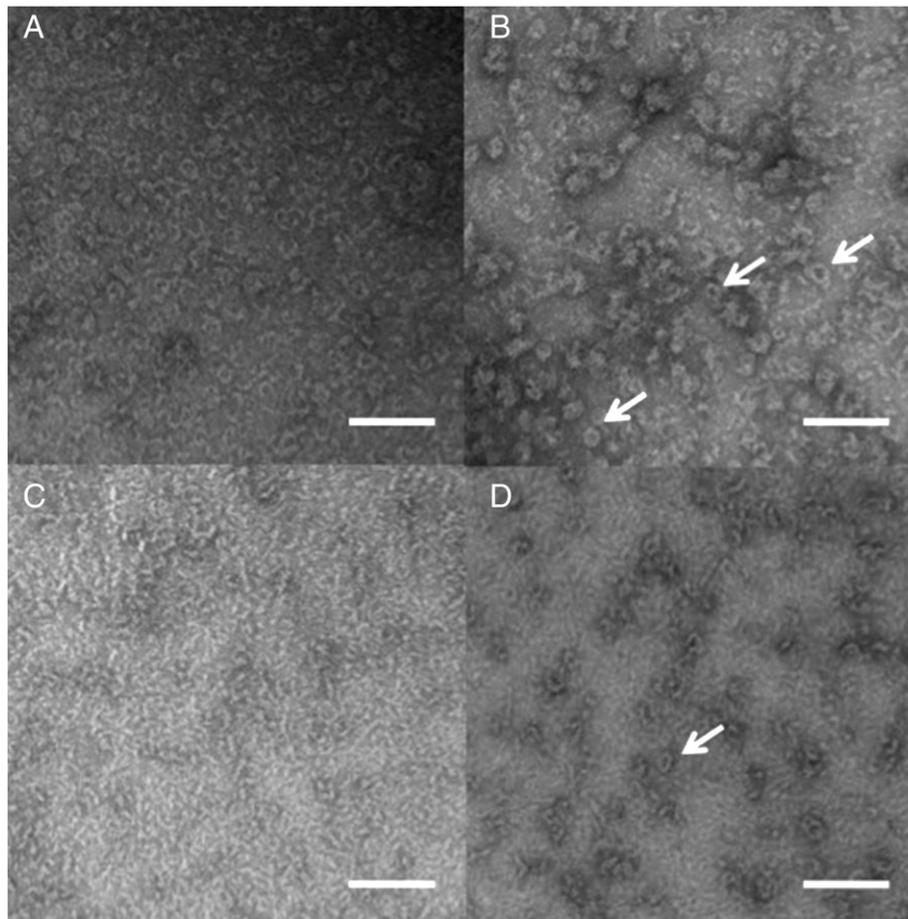
Fig. 2. TEM images of wt-Dyn2 (A) and R369W (B) showing assembly into similar, though not identical, ring structures under low salt conditions (50 mM NaCl). WT-Dyn2 (C) shows diminished polymerization in the presence of GTP (2 mM), whereas R369W polymers are less affected by nucleotide (D). Arrows show R369W rings and scale bars denote 200 nm.

other in vitro analyses have indicated that unassembled wt dynamins are exclusively tetrameric [35] or predominantly dimeric [36]. Here we performed brightness analysis of FFS data (see Experimental Procedures) to determine the average oligomeric states of wt and R369W forms of Dyn2-EGFP as a function of their concentrations in the cytoplasm of U2OS cells. We have confirmed that EGFP fused to the C-terminus of Dyn2 does not alter its in vitro properties [37]. As shown in Fig. 4, at lower concentrations, wt-Dyn2 appears to be present in the cytosol as oligomers smaller than tetramers, but at concentrations approaching 2 μM it is predominantly tetrameric, and its average oligomeric state increases only slightly at higher concentrations. In contrast, Dyn2-R369W self-associates into much higher-order oligomers, up to 12–14-mers, at cytosolic concentrations above ~1 μM.

3.4. Dyn2-R369W forms larger and more stable clathrin-containing complexes on the plasma membrane than wt-Dyn2

We next sought to determine if the R369W mutation affected the size of clathrin-coated structures on the plasma membrane (PM). We previously used FFS in the TIRF mode to demonstrate that unassembled wt-Dyn2 is predominantly tetrameric on the PM [38]. In the present study, MEFs were transfected with wt-Dyn2-EGFP or R369W-EGFP alone, or together with clathrin light chain a (LCa)-mCherry. Fig. 5A and B show cells expressing either wt-Dyn2 or the R369W mutant, respectively. The average sizes of the Dyn2-containing puncta were determined using the spatial autocorrelation function (ACF) as described in Experimental Procedures. The spatial ACF was then fit to a Gaussian model. ACFs for cells expressing Dyn2-EGFP or R369W-EGFP are shown in Fig. 5C and D, respectively. The distribution of ACF sizes found for both cases are shown in Fig. 5E. The average size of the puncta containing wt-Dyn2 was 0.23 μm, which is approximately the size of the diffraction limited spot (PSF) in our microscope and, hence, represents an upper limit of their true size. In contrast, puncta containing the R369W mutant were unambiguously larger than the PSF of the microscope, indicating that the mutant forms large structures. Co-expression of LCa-mCherry did not alter the sizes of the Dyn2 puncta and the ACF for LCa-mCherry was found to be equal to or larger than wt-Dyn2 (range 0.2–0.25 μm, n = 5) and R369W (range 0.48–1.03 μm, n = 7) puncta. We also observed in these experiments that almost every R369W punctum contains clathrin, whereas many wt-Dyn2 puncta did not co-localize with clathrin (data not shown).

As shown in the intensity versus brightness histograms (Fig. 5F), cells expressing the R369W mutant contain more pixels corresponding to very high brightness levels, whereas cells expressing wt-Dyn2 contain more pixels corresponding to intermediate brightness levels. We suggest that the wt-Dyn2 pixels of intermediate brightness levels correspond to the assembly of "normal" dynamin collars and that these normal collars are greatly reduced in the case of the R369W mutant, which instead incorporate into large complexes, which we believe represent the stabilized dynamin polymers.

Another difference between wt and mutant forms of Dyn2 relates to the temporal behavior of the punctal intensity. When visualized at 100 frames/s for a total of 1000 frames, the flickering, or fluctuation, in the brightness of wt-Dyn2 puncta was larger than that of R369W (data not shown). However, we also noticed that the fluctuations of R369W-containing puncta were not only smaller than those displayed by wt-Dyn2, but were also slower (not shown), further suggesting
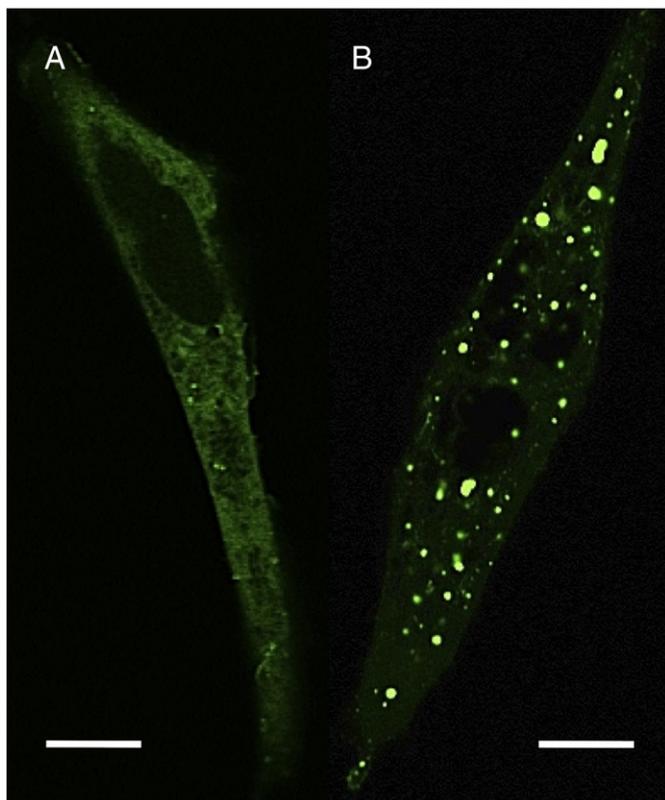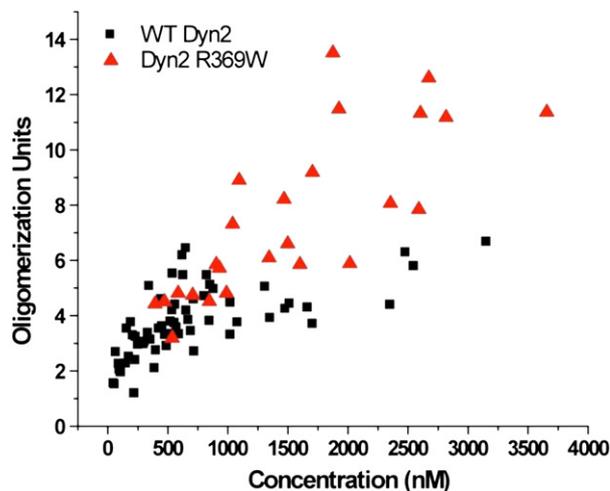
Fig. 3. Confocal fluorescence images of CV1 cells transfected with wt-Dyn2-EGFP (A) and R369W-EGFP (B). Scale bar denotes 10 μm.

Fig. 4. Oligomeric states of wt-Dyn2-EGFP (black) and R369W-EGFP (red) in the cytosol of U2OS cells as a function of concentration. Monomeric EGFP in U2OS cells was used as the standard (data not shown).

that the R369W clusters on the PM are more stable than those of wt-Dyn2.

4. Discussion

This report was based on our previous study [20], and that of Kenniston and Lemmon [21], showing that CNM-causing mutations enhance Dyn2 self-assembly. We focused primarily on the R369W middle domain mutant, first described by Bitoun et al. in 2005 [6] and to date identified in 10 families with childhood/adult onset CNM [19]. Electron micrographs indicated that this mutant is capable of forming rings that are stable even in the presence of GTP (Fig. 2), consistent with our prior finding that R369W polymers are more resistant to GTP-dependent disassembly than wt-Dyn2 polymers [20]. In the cytoplasm of living cells, Dyn2-R369W formed larger low-order, i.e., pre-assembly, oligomers than wt-Dyn2, which was predominantly tetrameric, although at lower concentrations there were apparently smaller oligomeric species. These smaller species could reflect the tetramer to monomer equilibrium we had previously reported based on analytical ultracentrifugation studies [30–32]. However, it is also possible that the oligomeric states recorded at low concentrations may be underestimated due to the presence of endogenous "dark" Dyn2 co-oligomerizing with the EGFP-tagged proteins. As demonstrated by TIRF/FFS experiments, the R369W mutant also formed larger and more stable structures than wt-Dyn2 on the plasma membrane of living cells. Unlike wt-Dyn2, nearly the entire PM pool of Dyn2-R369W co-localized with clathrin, perhaps explaining the reported deficiency in clathrin-independent endocytosis in cells expressing CNM mutant Dyn2 [39]. Interestingly, it was previously shown that the R369W mutant is less abundant on centrosomes than wt-Dyn2 [6] and that other CNM-linked mutants were relatively depleted from microtubules [31], the trans-Golgi network [39], and PDGF-induced dorsal ruffles [39].

The greater size of clathrin/R369W-containing puncta, compared to clathrin/wt-Dyn2-containing puncta, may be explained by at least two models, both of which take into account our finding that clathrin extends beyond (or surrounds) Dyn2 in these puncta. As reviewed in [40], a heterogeneous population of clathrin-coated structures are formed on the PM, including "abortive clathrin coats", which have lifetimes of <20 s and do not invaginate or develop into vesicles, "canonical" coated pits, which are small (diffraction limited) structures that accumulate proteins for ~1 min and then rapidly internalize as clathrin-coated vesicles, and "coated plaques", which are larger structures (often above the diffraction limit) with longer lifetimes (~2–15 min). Our data are consistent with the association of wt-Dyn2 with abortive and/or canonical clathrin-coated structures, and with the preferential formation of coated plaques by the R369W mutant. In model A (Fig. 6A), the R369W mutation would allow Dyn2 to circumvent its reported requirement of high membrane curvature for membrane scission [41], perhaps resulting in the formation of inordinately large endocytic vesicles. In model B (Fig. 6B) the high curvature requirement for Dyn2-dependent membrane scission is retained by the R369W mutant, leading to the emergence of multiple "canonical" clathrin-coated vesicles from the plaque-like structure. These "cactus-like" structures have been observed by Takei et al. [43], who noted their formation in cells treated with GTPγS, a very slowly hydrolysable GTP analog. In the absence of GTP hydrolysis, dynamin collars will not disassemble, a situation that may resemble the case of the R369W mutant.

At present it is not entirely clear how CNM-mutant forms of Dyn2 affect clathrin-mediated endocytosis (CME). The majority of studies have focused on effects of R465W, the most frequently found CNM-linked mutation. For example, transferrin uptake was found to be inhibited in COS cells overexpressing the R465W mutant [31,42]. Interestingly, when measured after 5 min of uptake, transferrin endocytosis was reduced in fibroblasts from a CNM patient expressing Dyn2-R465W [42], but no effect was seen in fibroblasts from other R465W-expressing patients when uptake was allowed to proceed for 15 min [31]. Therefore, as noted by Koutsopoulos et al. [31], the combined results of the two studies may suggest that the R465W mutation delays CME but does not block it entirely. CME was also inhibited in fibroblasts from mouse embryos homozygously expressing R465W, but not in fibroblasts from heterozygous mice [30]. This result may explain the failure of the homozygous mice to survive, and supports the view that CME defects are not detectable in cells expressing equal levels of wt and mutant forms of Dyn2 (see also [39]).

Recent structural analyses [44,45] have suggested a mechanism for the stabilization of dynamin polymers by CNM-associated mutations. These studies, together with previous x-ray crystallographic [46] and cryo-electron microscopic [47] investigations, indicate that the middle
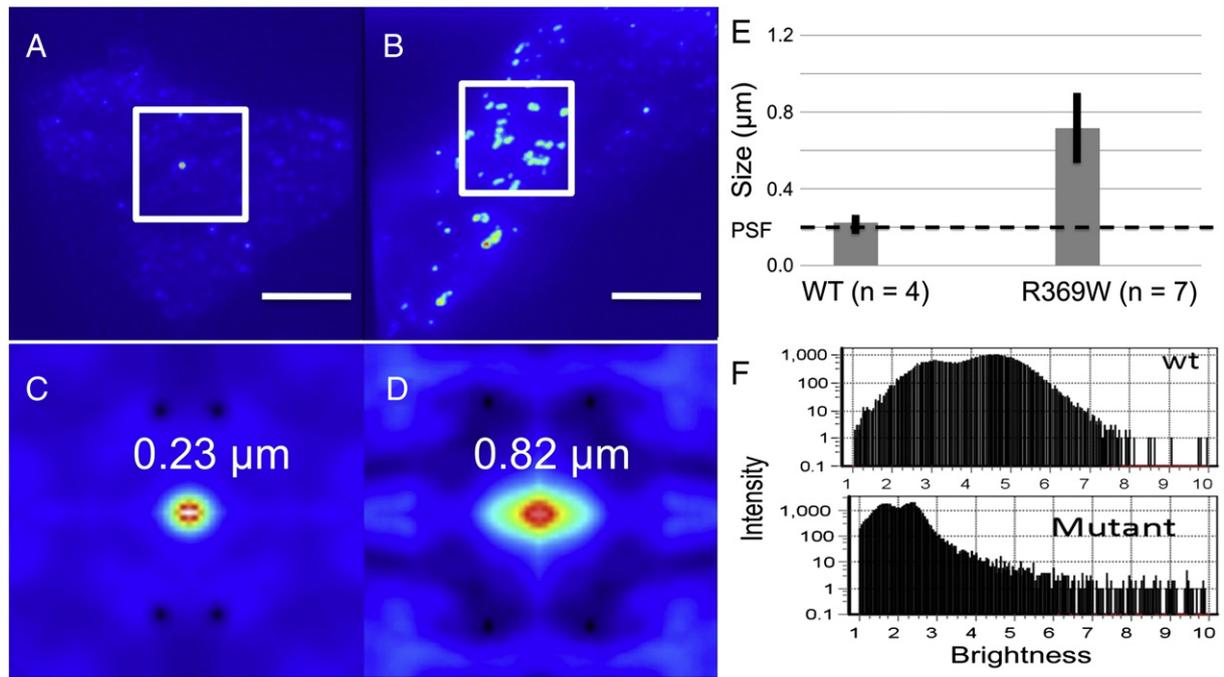
Fig. 5. (A and B) TIRF images of MEF cells expressing wt-Dyn2-EGFP and R369W-EGFP. Two intensity averaged cells are shown for each construct. The scale bar in the lower corner of each image is 10 μm. (C and D) Spatioautocorrelation (ACF) of TIRF images, seen in A and B, respectively. The ACF were fitted using a Gaussian model and the standard deviation of the fits, along with the average width of the puncta, is shown for each ACF. (E) Histogram of the average punctal size for wt-Dyn2 and R369W. The standard deviation for each is shown (black line) along with the size of the PSF (dashed line). (F) Histograms from images of cells expressing wt-Dyn2-EGFP or R369W-EGFP showing pixel numbers corresponding to different brightness levels.

domain and the GED comprise a "stalk" that participates in intermolecular interactions that are critical for dynamin self-assembly. Mutations in arginines 361, 386, or 399 in the middle domain inhibit oligomerization and assembly-dependent GTPase activation of dynamin 1 [48,49]. The PH domain, located between the middle domain and the GED, is connected to these two domains by flexible, unstructured loops. As evident in the crystal structures [44,45], these loops allow the PH domain to fold back and contact the middle domain, thereby blocking stalk-stalk interactions and suppressing dynamin assembly. Thus, the PH domain may participate in an intramolecular auto-inhibitory mechanism to prevent excessive dynamin polymerization [21]. This mechanism is apparently circumvented by mutations that weaken the interaction between the middle and PH domains. Interestingly, CNM-associated mutations that were found to inordinately stabilize dynamin polymers [20,21] are located in the contact interface between these two domains [44,45]. Based on crystallographic evidence, the R369W mutation examined in
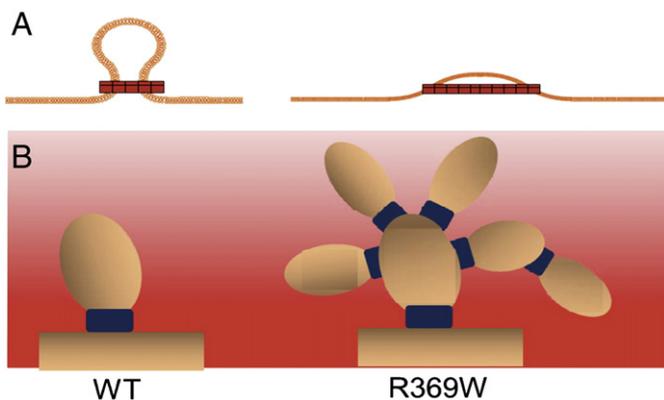
the present study would disrupt an interaction that normally occurs between R369 in the middle domain and E611 in the PH domain, in the folded-back, assembly-inhibited dynamin conformation.

Fig. 6. Representation of two potential mechanisms of assembly of wt and R369W Dyn2 on the plasma membrane. (A) WT-Dyn2 (left) requires highly curved membranes as templates of self-assembly [41], whereas the R369W mutant circumvents this requirement and assembles on relatively flat surfaces. (B) WT-Dyn2 preferentially promotes the formation of single clathrin-coated vesicle, whereas the R369W mutant induces clustering of coated vesicles prior to budding.

References

[1] N.B. Romero, Centronuclear myopathies: a widening concept, Neuromuscul. Disord. 20 (2010) 223–228.
[2] H. Jungbluth, C. Wallgren-Pettersson, J. Laporte, Centronuclear (myotubular) myopathy, Orphanet J. Rare Dis. 3 (2008) 26.
[3] J.J. Dowling, E.M. Gibbs, E.L. Feldman, Membrane traffic and muscle: lessons from human disease, Traffic 9 (2008) 1035–1043.
[4] J. Laporte, L.J. Hu, C. Kretz, J.L. Mandel, P. Kioschis, J.F. Coy, S.M. Klauck, A. Poustka, N. Dahl, A gene mutated in X-linked myotubular myopathy defines a new putative tyrosine phosphatase family conserved in yeast, Nat. Genet. 13 (1996) 175–182.
[5] A.S. Nicot, A. Toussaint, V. Tosch, C. Kretz, C. Wallgren-Pettersson, E. Iwarsson, H. Kingston, J.M. Garnier, V. Biancalana, A. Oldfors, J.L. Mandel, J. Laporte, Mutations in amphiphysin 2 (BIN1) disrupt interaction with dynamin 2 and cause autosomal recessive centronuclear myopathy, Nat. Genet. 39 (2007) 1134–1139.
[6] M. Bitoun, S. Maugenre, P.Y. Jeannet, E. Lacene, X. Ferrer, P. Laforet, J.J. Martin, J. Laporte, H. Lochmuller, A.H. Beggs, M. Fardeau, B. Eymard, N.B. Romero, P. Guicheney, Mutations in dynamin 2 cause dominant centronuclear myopathy, Nat. Genet. 37 (2005) 1207–1209.
[7] A.C. Durieux, B. Prudhon, P. Guicheney, M. Bitoun, Dynamin 2 and human diseases, J. Mol. Med. (Berl.) 88 (2010) 339–350.
[8] R. Ramachandran, Vesicle scission: dynamin, Semin. Cell Dev. Biol. 22 (2011) 10–17.
[9] S.L. Schmid, V.A. Frolov, Dynamin: functional design of a membrane fission catalyst, Annu. Rev. Cell Dev. Biol. 27 (2011) 79–105.
[10] S.M. Ferguson, P. De Camilli, Dynamin, a membrane-remodelling GTPase, Nat. Rev. Mol. Cell Biol. 13 (2012) 75–88.
[11] A.M. van der Bliek, E.M. Meyerowitz, Dynamin-like protein encoded by the Drosophila shibire gene associated with vesicular traffic, Nature 351 (1991) 411–414.
[12] S.M. Jones, K.E. Howell, J.R. Henley, H. Cao, M.A. McNiven, Role of dynamin in the formation of transport vesicles from the trans-Golgi network, Science 279 (1998) 573–577.

[13] E.S. Gold, D.M. Underhill, N.S. Morrissette, J. Guo, M.A. McNiven, A. Aderem, Dynamin 2 is required for phagocytosis in macrophages, J. Exp. Med. 190 (1999) 1849–1856.

[14] D.A. Schafer, Regulating actin dynamics at membranes: a focus on dynamin, Traffic 5 (2004) 463–469.

[15] H. Cao, F. Garcia, M.A. McNiven, Differential distribution of dynamin isoforms in mammalian cells, Mol. Biol. Cell 9 (1998) 2595–2609.

[16] S.M. Ferguson, G. Brasnjo, M. Hayashi, M. Wolfel, C. Collesi, S. Giovedi, A. Raimondi, L.W. Gong, P. Ariel, S. Paradise, E. O'Toole, R. Flavell, O. Cremona, G. Miesenbock, T.A. Ryan, P. De Camilli, A selective activity-dependent requirement for dynamin 1 in synaptic vesicle endocytosis, Science 316 (2007) 570–574.

[17] E. Smirnova, D.L. Shurland, E.D. Newman-Smith, B. Pishvaee, A.M. van der Bliek, A model for dynamin self-assembly based on binding between three different protein domains, J. Biol. Chem. 274 (1999) 14942–14947.

[18] J.S. Chappie, S. Acharya, Y.W. Liu, M. Leonard, T.J. Pucadyil, S.L. Schmid, An intramolecular signaling element that modulates dynamin function in vitro and in vivo, Mol. Biol. Cell 20 (2009) 3561–3571.

[19] J. Bohm, V. Biancalana, E.T. Dechene, M. Bitoun, C.R. Pierson, E. Schaefer, H. Karasoy, M.A. Dempsey, F. Klein, N. Dondaine, C. Kretz, N. Haumesser, C. Poirson, A. Toussaint, R.S. Greenleaf, M.A. Barger, L.J. Mahoney, P.B. Kang, E. Zanoteli, J. Vissing, N. Witting, A. Echaniz-Laguna, C. Wallgren-Pettersson, J. Dowling, L. Merlini, A. Oldfors, L. Bomme Ousager, J. Melki, A. Krause, C. Jern, A.S. Oliveira, F. Petit, A. Jacquette, A. Chaussenot, D. Mowat, B. Leheup, M. Cristofano, J.J. Poza Aldea, F. Michel, A. Furby, J.E. Llona, R. Van Coster, E. Bertini, J.A. Urtizberea, V. Drouin-Garraud, C. Beroud, B. Prudhon, M. Bedford, K. Mathews, L.A. Erby, S.A. Smith, J. Roggenbuck, C.A. Crowe, A. Brennan Spitale, S.C. Johal, A.A. Amato, L.A. Demmer, J. Jonas, B.T. Darras, T.D. Bird, M. Laurino, S.I. Welt, C. Trotter, P. Guicheney, S. Das, J.L. Mandel, A.H. Beggs, J. Laporte, Mutation spectrum in the large GTPase dynamin 2, and genotype–phenotype correlation in autosomal dominant centronuclear myopathy, Hum. Mutat. 33 (2012) 949–959.

[20] L. Wang, B. Barylko, C.E. Byers, J.A. Ross, D.M. Jameson, J.P. Albanesi, Dynamin 2 mutants linked to centronuclear myopathies form abnormally stable polymers, J. Biol. Chem. 285 (2010) 22753–22757.

[21] J.A. Kenniston, M.A. Lemmon, Dynamin GTPase regulation is altered by PH domain mutations found in centronuclear myopathy patients, EMBO J. 29 (2010) 3054–3067.

[22] N. Hanna, R. Bouhenni, B. Gupta, K.K. Abu-Amero, R. Wollmann, D.P. Edward, Histopathologic changes in the extraocular muscle in centronuclear myopathy with a dynamin 2 mutation, Ophthalmic Genet. 34 (2012) 83–86.

[23] H.C. Lin, B. Barylko, M. Achiriloaie, J.P. Albanesi, Phosphatidylinositol (4,5)-bisphosphate-dependent activation of dynamins I and II lacking the proline/arginine-rich domains, J. Biol. Chem. 272 (1997) 25999–26004.

[24] M.A. Digman, C.M. Brown, P. Sengupta, P.W. Wiseman, A.R. Horwitz, E. Gratton, Measuring fast dynamics in solutions and cells with a laser scanning microscope, Biophys. J. 89 (2005) 1317–1327.

[25] J.R. Unruh, E. Gratton, Analysis of molecular concentration and brightness from fluorescence fluctuation data with an electron multiplied CCD camera, Biophys. J. 95 (2008) 5385–5398.

[26] M.A. Digman, R. Dalal, A.F. Horwitz, E. Gratton, Mapping the number of molecules and brightness in the laser scanning microscope, Biophys. J. 94 (2008) 2320–2332.

[27] Y. Chen, L.N. Wei, J.D. Muller, Probing protein oligomerization in living cells with fluorescence fluctuation spectroscopy, Proc. Natl. Acad. Sci. U. S. A. 100 (2003) 15492–15497.

[28] A. Sanchez-Andres, Y. Chen, J.D. Muller, Molecular brightness determined from a generalized form of Mandel's Q-parameter, Biophys. J. 89 (2005) 3531–3547.

[29] J.E. Hinshaw, S.L. Schmid, Dynamin self-assembles into rings suggesting a mechanism for coated vesicle budding, Nature 374 (1995) 190–192.

[30] A.C. Durieux, A. Vignaud, B. Prudhon, M.T. Viou, M. Beuvin, S. Vassilopoulos, B. Fraysse, A. Ferry, J. Laine, N.B. Romero, P. Guicheney, M. Bitoun, A centronuclear myopathy-dynamin 2 mutation impairs skeletal muscle structure and function in mice, Hum. Mol. Genet. 19 (2010) 4820–4836.

[31] O.S. Koutsopoulos, C. Koch, V. Tosch, J. Bohm, K.N. North, J. Laporte, Mild functional differences of dynamin 2 mutations associated to centronuclear myopathy and Charcot–Marie–Tooth peripheral neuropathy, PLoS One 6 (2011) e27498.

[32] D.D. Binns, B. Barylko, N. Grichine, M.A. Atkinson, M.K. Helms, D.M. Jameson, J.F. Eccleston, J.P. Albanesi, Correlation between self-association modes and GTPase activation of dynamin, J. Protein Chem. 18 (1999) 277–290.

[33] J.F. Eccleston, D.D. Binns, C.T. Davis, J.P. Albanesi, D.M. Jameson, Oligomerization and kinetic mechanism of the dynamin GTPase, Eur. Biophys. J. 31 (2002) 275–282.

[34] B. Barylko, L. Wang, D.D. Binns, J.A. Ross, T.C. Tassin, K.A. Collins, D.M. Jameson, J.P. Albanesi, The proline/arginine-rich domain is a major determinant of dynamin self-activation, Biochemistry 49 (2010) 10592–10594.

[35] A.B. Muhlberg, D.E. Warnock, S.L. Schmid, Domain structure and intramolecular regulation of dynamin GTPase, EMBO J. 16 (1997) 6676–6683.

[36] P.L. Tuma, C.A. Collins, Activation of dynamin GTPase is a result of positive cooperativity, J. Biol. Chem. 269 (1994) 30842–30847.

[37] D.M. Jameson, N.G. James, J.P. Albanesi, Fluorescence fluctuation spectroscopy approaches to the study of receptors in live cells, Methods Enzymol. 519 (2013) 87–113.

[38] J.A. Ross, M.A. Digman, L. Wang, E. Gratton, J.P. Albanesi, D.M. Jameson, Oligomerization state of dynamin 2 in cell membranes using TIRF and number and brightness analysis, Biophys. J. 100 (2011) L15–L17.

[39] Y.W. Liu, V. Lukiyanchuk, S.L. Schmid, Common membrane trafficking defects of disease-associated dynamin 2 mutations, Traffic 12 (2011) 1620–1633.

[40] T. Kirchhausen, Imaging endocytic clathrin structures in living cells, Trends Cell Biol. 19 (2009) 596–605.

[41] Y.W. Liu, S. Neumann, R. Ramachandran, S.M. Ferguson, T.J. Pucadyil, S.L. Schmid, Differential curvature sensing and generating activities of dynamin isoforms provide opportunities for tissue-specific regulation, Proc. Natl. Acad. Sci. U. S. A. 108 (2011) E234–E242.

[42] M. Bitoun, A.C. Durieux, B. Prudhon, J.A. Bevilacqua, A. Herledan, V. Sakanyan, A. Urtizberea, L. Cartier, N.B. Romero, P. Guicheney, Dynamin 2 mutations associated with human diseases impair clathrin-mediated receptor endocytosis, Hum. Mutat. 30 (2009) 1419–1427.

[43] K. Takei, O. Mundigl, L. Daniell, P. De Camilli, The synaptic vesicle cycle: a single vesicle budding step involving clathrin and dynamin, J. Cell Biol. 133 (1996) 1237–1250.

[44] K. Faelber, Y. Posor, S. Gao, M. Held, Y. Roske, D. Schulze, V. Haucke, F. Noe, O. Daumke, Crystal structure of nucleotide-free dynamin, Nature 477 (2011) 556–560.

[45] M.G. Ford, S. Jenni, J. Nunnari, The crystal structure of dynamin, Nature 477 (2011) 561–566.

[46] S. Gao, A. von der Malsburg, S. Paeschke, J. Behlke, O. Haller, G. Kochs, O. Daumke, Structural basis of oligomerization in the stalk region of dynamin-like MxA, Nature 465 (2010) 502–506.

[47] P. Zhang, J.E. Hinshaw, Three-dimensional reconstruction of dynamin in the constricted state, Nat. Cell Biol. 3 (2001) 922–926.

[48] R. Ramachandran, M. Surka, J.S. Chappie, D.M. Fowler, T.R. Foss, B.D. Song, S.L. Schmid, The dynamin middle domain is critical for tetramerization and higher-order self-assembly, EMBO J. 26 (2007) 559–566.

[49] K. Takahashi, M. Otomo, N. Yamaguchi, H. Nakashima, H. Miyoshi, Replacement of Arg-386 with Gly in dynamin 1 middle domain reduced GTPase activity and oligomer stability in the absence of lipids, Biosci. Biotechnol. Biochem. 76 (2012) 2195–2200.